PHYSICAL REVIEW D **88,** 064004 (2013)

Shadow of rotating non-Kerr black hole

Farruh Atamurotov,[1,*] Ahmadjon Abdujabbarov,[1,2,†] and Bobomurat Ahmedov[1,2,3,‡]
[1]*Institute of Nuclear Physics, Ulughbek, Tashkent 100214, Uzbekistan*
[2]*Ulugh Beg Astronomical Institute, Astronomicheskaya 33, Tashkent 100052, Uzbekistan*
[3]*The Abdus Salam International Centre for Theoretical Physics, 34151 Trieste, Italy*
(Received 5 April 2013; published 3 September 2013)

The shadow of a rotating non-Kerr black hole has been studied, and it was shown that in addition to the specific angular momentum a, the deformation parameter of non-Kerr spacetime essentially deforms the shape of the black hole shadow. For a given value of the black hole spin parameter a, the presence of a deformation parameter ϵ reduces the shadow and enlarges its deformation with respect to the one in the Kerr spacetime. Optical features of the rotating non-Kerr black hole in terms of rotation of the polarization vector along null congruences have been studied. A comparison of the obtained theoretical results on the polarization angle with the observational data on Faraday rotation measurements provides the upper limit for the dimensionless deformation parameter as $\epsilon \leq 19$.

DOI: 10.1103/PhysRevD.88.064004 PACS numbers: 04.50.Kd, 04.70.−s, 04.25.−g

I. INTRODUCTION

Being apparently the simplest geometric theory of gravitation, in Einsteins general relativity, a number of fundamental problems regarding the nature of singularities, dark energy and dark matter, and quantization of gravitational interactions is appearing. To solve the mentioned problems, theorists are forced to use alternative theories of gravity (e.g., the so-called modified theories of gravity [1], higher-curvature [2], braneworld scenarios [3], etc.), which give the same observational consequences at the modern level of experiments. A future experimental test of the strong field regime may be given, for example, by gravitational interferometers, which could detect gravitational waves from neutron stars and black holes through, for example, observation of the quasinormal modes of these compact objects.

Recently a number of works has been devoted to the study of potentially observable processes around various non-Kerr black holes [4]. Therefore, a unified description of analogs of the Schwarzschild and Kerr solutions in various theories of gravity would be most useful for testing the alternatives to general relativity. Such a model was suggested by Johannsen and Psaltis [5], who considered deviations from the Schwarzschild and Kerr solutions and found a regular spacetime outside the event horizon, which reduces to the Kerr one, when the deformation parameters vanish. The Johannsen and Psaltis metric is not a vacuum solution of the Einstein equations but is obtained in a kind of perturbative way in order to include various possible deviations from the Kerr solution in alternative theories of gravity.

The Kerr nature of astrophysical black hole candidates can potentially be tested with already available x-ray data, by extending the technique called the continuum fitting method [6]. With the continuum fitting method, one can study the thermal spectrum of geometrically thin and optically thick accretion disks: under the assumption of Kerr background and with independent measurements of the mass of the object, its distance from us, and the inclination angle of the disk, it is possible to infer the spin parameter a and the mass accretion rate $\dot{M}$. Note that one can usually get only a constraint on a certain combination of the spin parameter and of the deviations from the Kerr background. In order to really test the nature of the compact object, at least two independent measurements are necessary [7].

In the recent paper [8], the properties of the ergosphere and energetic processes in spacetime of a rotating non-Kerr black hole have been investigated. Direct imaging of rapidly rotating non-Kerr black holes and their shadows are recently studied in the paper [9]. Strong gravitational lensing by a rotating non-Kerr compact object are investigated in Ref. [10]. The strong dependence of the predicted energy spectra and energy-dependent polarization degree and polarization direction on the parameters of a rotating non-Kerr black hole is found in Ref. [11]. The brief review on testing the Kerr black hole hypothesis is given in Ref. [12]. The accretion disc properties around rotating non-Kerr compact object can provide the observational signature to distinguish it from the Kerr black hole [13].

Although a black hole is not visible, it may be observable nonetheless since it may create a shadow if it is in front of a bright background. The apparent shape of an extremely rotating black hole was first studied by Bardeen [14]; later a Schwarzschild black hole with an accretion disk was visualized by Luminet [15]. Accretion discs around an extremely rotating black hole as viewed from different angles of latitude were investigated in detail in Ref. [16]. Supplementing these numerical approaches, the closed photon orbits in general Kerr-Newman spacetimes were analytically studied in Ref. [17], even in cases where the so-called cosmic censorship is violated. It is strongly

*farruh@astrin.uz
†ahmadjon@astrin.uz
‡ahmedov@astrin.uz

believed that the observability of black hole shadows in the near future is very realistic [18]. Recently, great interest emerged especially for the observability of the black hole in the center of Milky Way, Sgr A* [19]. The shadow of Schwarzschild [20,21], rotating black hole with gravitomagnetic charge [22], Reissner-Nordström [23], and other spherically symmetric black holes [24] have been intensively studied. Nonrotating braneworld black holes were studied as gravitational lenses [25] as well. The shadow cast by a rotating braneworld black hole was studied in Ref. [26] in the Randall-Sundrum scenario.

Kerr black holes as gravitational lenses were studied by many authors; see, for example, Refs. [27–30]. Rotating black holes present apparent shapes or shadows with an optical deformation due to the spin [31,32], instead of being circles as in the case of nonrotating ones. This topic has been reexamined by several authors in the last few years [18,29,33–35], with the expectation that the direct observation of black holes will be possible in the near future [35]. Therefore, the study of the shadows could be useful for measuring the properties of astrophysical black holes. Optical properties of rotating braneworld black holes were studied by Schee and Stuchlik [36]. For more details about black hole gravitational lensing and a discussion of its observational prospects, see the recent review article, Ref. [37], and the references therein.

The other aim of this paper is to study the optical features of the rotating non-Kerr black hole. Following Ref. [38], we have used the Newman-Penrose formalism [39] adapted to the locally nonrotating frames [40] to obtain the rotation of the polarization vector of the light in the geometrical optics regime, which is appropriate for high-frequency electromagnetic waves. In this approach, the light propagates along null geodesics, and its polarization vector is parallelly transported.

The paper is organized as follows. In Sec. II, we review the basic aspects of the geometry and the geodesics around the non-Kerr black hole. In Sec. III, we obtain the shadows of black holes with different values of the black hole's spin parameter a and parameters of non-Kerr spacetime. Section IV is devoted to study the rotation of polarization vector for non-Kerr black hole. Finally, in Sec. V we discuss the results obtained.

Throughout the paper, we use a spacelike signature $(-,+,+,+)$ and a system of units in which $G = 1 = c$. (However, for those expressions with an astrophysical application, we have written the speed of light explicitly.) Greek indices are taken to run from 0 to 3 and Latin indices from 1 to 3; covariant derivatives are denoted with a semicolon and partial derivatives with a comma.

II. GEODESIC EQUATIONS OF ROTATING NON-KERR BLACK HOLES

The deformed Kerr-like metric, which describes a stationary axisymmetric and asymptotically flat vacuum spacetime in the standard Boyer-Lindquist coordinates, can be expressed as [5]

$$\begin{aligned} ds^2 = &-\left(1-\frac{2Mr}{\Sigma^2}\right)(1+h)dt^2 + \frac{\Sigma^2(1+h)}{\Delta + a^2 h \sin^2\theta}dr^2 \\ &+ \Sigma^2 d\theta^2 - \frac{4aMr\sin^2\theta}{\Sigma^2}(1+h)dtd\phi \\ &+ \sin^2\theta\left[\Sigma^2 + \frac{a^2(\Sigma^2+2Mr)\sin^2\theta}{\Sigma^2}(1+h)\right]d\phi^2, \end{aligned} \tag{1}$$

where

$$\Sigma^2 = r^2 + a^2\cos^2\theta, \qquad \Delta = r^2 - 2Mr + a^2.$$

Together with the mass and spin of the black hole, this spacetime metric contains parameters that measure potential deviations from the Kerr metric and reduces to the Kerr metric in Boyer-Lindquist coordinates in the case when $h(r) = 0$. The function $h(r)$ can be chosen as

$$h(r) = \sum_{k=0}^{\infty} \epsilon_k \left(\frac{M}{r}\right)^k,$$

and the constraints on ϵ_k can be found from asymptotical properties of the metric (1). In the limit of large radii, the stationary and asymptotically flat spacetimes are Schwarzschild-like [41]:

$$\begin{aligned} ds^2 = &-\left(1-\frac{2M}{r}+\mathcal{O}(r^{-2})\right)dt^2 - \left(\frac{4a}{r}\sin^2\theta + \mathcal{O}(r^{-2})\right)dtd\phi \\ &+ (1+\mathcal{O}(r^{-1}))(dr^2 + r^2 d\theta^2 + \sin^2\theta d\phi^2). \end{aligned} \tag{2}$$

In the $r \to \infty$ limit, the metric (1) will take the following form:

$$\begin{aligned} ds^2 = &-\left(1-\frac{2M}{r}+h(r)\right)dt^2 - \frac{4a(1+h(r))}{r}\sin^2\theta dtd\phi \\ &+ \left(1+\frac{2M}{r}+h(r)\right)dr^2 + r^2 d\theta^2 + \sin^2\theta d\phi^2. \end{aligned} \tag{3}$$

The requirement of the asymptotic flatness of the metric implies that $\epsilon_0 = \epsilon_1 = 0$. In the parametrized post-Newtonian (PPN) approach [42], the asymptotic spacetime is expressed in the form

$$\begin{aligned} ds^2 = &-\left(1-\frac{2M}{r}+2(\beta-\gamma)\frac{M^2}{r^2}\right)dt^2 + \left(1+2\gamma\frac{M}{r}\right)dr^2 \\ &+ r^2 d\theta^2 + \sin^2\theta d\phi^2, \end{aligned} \tag{4}$$

where β and γ are the dimensionless PPN parameters. Comparision the constraint on β obtained from the Lunar Laser Ranging experiment [43] as

$$|\beta - 1| \leq 2.3 \times 10^{-4}$$

and asymptotical expression of metric (1) given in Eq. (3) provide the vanishing value of $\epsilon_2 = 0$. Thus, our choice of the function $h(r)$ to be the third power of M/r as in Ref. [5] is

$$h(r,\theta) = \epsilon_3 \frac{M^3 r}{\Sigma^4}.$$

Further in the text, we drop the index 3 and use the parameter ϵ as deformation parameter. The quantity $\epsilon > 0$ or $\epsilon < 0$ corresponds to the cases in which the event horizon of compact object is more prolate or oblate than that of the Kerr black hole, respectively. As $\epsilon = 0$, the black hole is reduced to the typical Kerr black hole well known in general relativity.

Note that the spacetime metric (1) is stationary and axisymmetric, and chosen $h(r,\theta)$ ensures the preservation of the properties of the Kerr metric. In general relativity, the Einstein tensor of spacetime metric (1) is nonzero for nonvanishing $h(r,\theta)$. One should regard the spacetime metric (1) as a vacuum spacetime of modified set of field equations which are unknown but different from the Einstein equations for nonzero $h(r,\theta)$.

Suppose a black hole is placed between a source of light and an observer. The light reaches the observer after being deflected by the rotating black hole's gravitational field. But some part of the deflected light with small impact parameters can be absorbed by the central black hole. This phenomenon results in a dark figure in the map of the space called the shadow. The boundary of this shadow defines the shape of a black hole (see, e.g., Ref. [26]). The study of the geodesic structure around the black hole is very important to obtain the apparent shape. The Hamilton-Jacobi equation determines the geodesics for a given spacetime geometry:

$$\frac{\partial S}{\partial \lambda} = -\frac{1}{2} g^{\mu\nu} \frac{\partial S}{\partial x^\mu} \frac{\partial S}{\partial x^\nu}, \tag{5}$$

where λ is an affine parameter along the geodesics, $g_{\mu\nu}$ are the components of the metric tensor, and S is the Jacobi action. If the problem is separable, the Jacobi action S can be written in the form

$$S = \frac{1}{2} m^2 \lambda - \mathcal{E} t + \mathcal{L}\phi + S_r(r) + S_\theta(\theta), \tag{6}$$

where m is the mass of a test particle. The second term in the right-hand side is related to the conservation of energy $\mathcal{E}$, while the third term is related to the conservation of the angular momentum $\mathcal{L}$ in the direction of the axis of symmetry. In the case of null geodesics, we have that $m = 0$, and from the Hamilton-Jacobi equation, the following equations of motion are obtained:

$$\Sigma^2 \frac{dt}{d\lambda} = \frac{r^2 + a^2}{\Delta + a^2 h \sin^2\theta}[(r^2 + a^2)\mathcal{E} - a\mathcal{L}] + \frac{\Delta a}{\Delta + a^2 h \sin^2\theta}[\mathcal{L} - a\mathcal{E}\sin^2\theta], \tag{7}$$

$$\Sigma^2 \frac{d\phi}{d\lambda} = \frac{a}{\Delta + a^2 h \sin^2\theta}[(r^2 + a^2)\mathcal{E} - a\mathcal{L}] + \frac{\Delta}{\Delta + a^2 h \sin^2\theta}\left[\frac{\mathcal{L}}{\sin^2\theta} - a\mathcal{E}\right], \tag{8}$$

$$\frac{\Sigma^2}{1+h}\frac{dr}{d\lambda} = \sqrt{\mathcal{R}}, \tag{9}$$

$$\Sigma^2 \frac{d\theta}{d\lambda} = \sqrt{\Theta}, \tag{10}$$

where the functions $\mathcal{R}(r)$ and $\Theta(\theta)$ are defined as

$$\mathcal{R} = [(r^2 + a^2)\mathcal{E} - a\mathcal{L}]^2 - \Delta[\mathcal{K} + (\mathcal{L} - a\mathcal{E})^2], \tag{11}$$

$$\Theta = \mathcal{K} - \frac{\Sigma^2}{\sin^2\theta}[a\mathcal{E}\sin^2\theta - \mathcal{L}]^2, \tag{12}$$

with $\mathcal{K}$ as Carter constant of separation.

In Fig. 1 the radial dependence of the effective potential of the massless particle's radial motion is shown. When $\epsilon < 0$ with decreasing the value of deformation parameter, one may observe the increase of the photon sphere. The stability of circular orbits is decreasing with the increase in the module of negative ϵ. From this dependence one can easily see that with the increase of the ϵ parameter, stable circular photon orbits come closer to the central object.

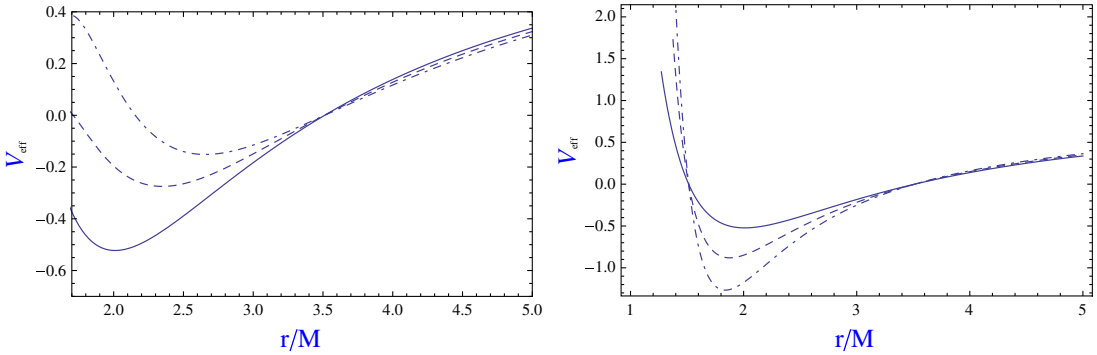

FIG. 1 (color online). The radial dependence of the effective potential of radial motion of the massless particles for the different values of the ϵ parameter: solid line for $\epsilon = 0$, dashed line for $\epsilon = -5$, and dotted-dashed line for $\epsilon = -10$ (left panel) and solid line for $\epsilon = 0$, dashed line for $\epsilon = 5$, and dotted-dashed line for $\epsilon = 10$ (right panel).

Then the stability of photon orbits will also increase with the increase of the parameter ϵ. The similar effect for the particle motion around rotating non-Kerr black hole has been found in Ref. [44], where it was shown that with the increase of the parameter ϵ, the radius of the innermost stable circular orbits at the equatorial plane is decreasing.

Equations (7)–(10) determine the propagation of light in the non-Kerr spacetime (1). The light rays are in general characterized by two impact parameters which can be expressed in terms of the constants of motion $\mathcal{E}$, $\mathcal{L}$, and the Carter constant $\mathcal{K}$. Combining these quantities we define as usual $\xi = \mathcal{L}/\mathcal{E}$ and $\eta = \mathcal{K}/\mathcal{E}^2$, which are the impact parameters for general orbits around the black hole. We use Eq. (9) to derive the orbits with constant r in order to obtain the boundary of the shadow of the black hole. These orbits satisfy the conditions $\mathcal{R}(r) = 0 = d\mathcal{R}(r)/dr$, which are fulfilled by the values of the impact parameters that determine the contour of the shadow, namely,

$$\xi(r) = \frac{a^2(1+r) + r^2(r-3)}{a(1-r)}, \tag{13}$$

$$\eta(r) = \frac{r^3[4a^2 - r(r-3)^2]}{a^2(1-r)^2}. \tag{14}$$

In expressions (13) and (14) we put $M = 1$ for simplicity.

III. SHADOW OF ROTATING NON-KERR BLACK HOLE

Using the celestial coordinates, one can easily describe the shadow (see, for example, Ref. [28]):

$$\alpha = \lim_{r_0 \to \infty}\left(-r_0^2 \sin\theta_0 \frac{d\phi}{dr}\right) \tag{15}$$

and

$$\beta = \lim_{r_0 \to \infty} r_0^2 \frac{d\theta}{dr}, \tag{16}$$

since here an observer far away from the black hole is considered at $r_0 \to \infty$; θ_0 is the angular coordinate of the observer, i.e., the inclination angle between the rotation axis of the black hole and the line of sight of the observer. The geometry of the introduced new coordinates is shown in Fig. 2. The coordinates α and β are the apparent perpendicular distances of the image as seen from the axis of symmetry and from its projection on the equatorial plane, respectively.

Calculating $d\phi/dr$ and $d\theta/dr$ using the spacetime metric given by expression (1) and taking the coordinate's limit of a far away observer, one can obtain celestial coordinates functions of the constants of motion in the form

$$\alpha = -\frac{\Delta}{\Delta + a^2 h \sin^2\theta}\xi \csc\theta_0, \tag{17}$$

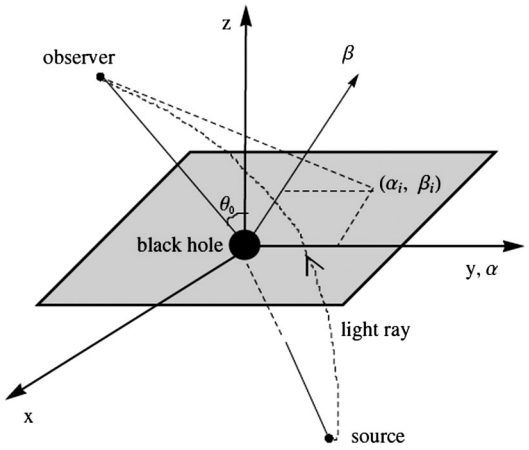

FIG. 2. The schematic geometry of the gravitational lens. An observer far away from the black hole can set up a reference coordinate system (x, y, z) with the black hole at the origin. The Boyer-Lidquist coordinates coincide with this system only at infinity. The tangent vector to an incoming light ray defines a straight line which intersects the α-β plane at the point (α_i, β_i).

$$\beta = \pm\sqrt{\eta + a^2\cos^2\theta_0 - \xi\cot^2\theta_0}, \tag{18}$$

where Eqs. (8)–(10), was used to calculate $d\theta/dr$ and $d\phi/dr$. These equations have implicitly the same form as the one for the Kerr spacetime metric with the new parameters ξ and η given by Eqs. (13) and (14) (a detailed calculation of the values of ξ and η and the expressions of the celestial coordinates α and β as a function of the constants of motion for the Kerr geometry are given in Ref. [28]).

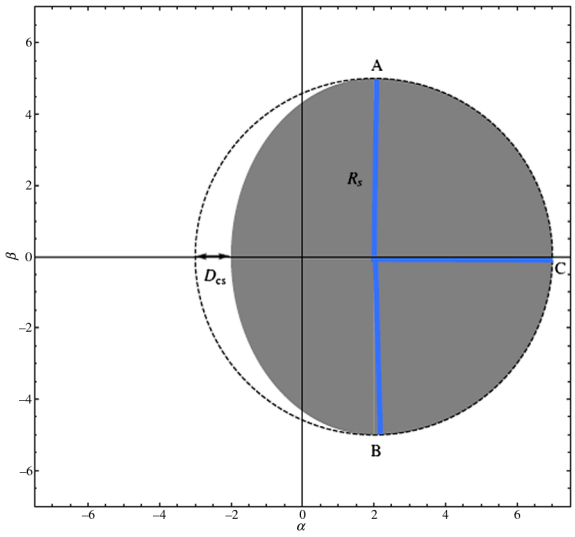

FIG. 3 (color online). The observables for the apparent shape of a rotating black hole are the radius R_s and the distortion parameter $\delta_s = D_{cs}/R_s$. Here D_{cs} is the difference between the left endpoints of the circle and of the shadow.

In the case of rotating black hole, one may introduce two observables which approximately characterize the apparent shape. First, one should approximate the apparent shape by a circle passing through three points which are located at the top position, bottom, and the most right end of the shadow as shown in Fig. 3. The radius R_s of the shadow is defined by the radius of this circle. One can also define the distortion parameter δ_s of the black hole shadow as $\delta_s = D_{cs}/R_s$. Two variables (R_s and δ_s) can be interpreted as observables in astronomical observation [18].

When the observer is situated in the equatorial plane of the black hole, the inclination angle is $\theta_0 = \pi/2$, and the gravitational effects on the shadow, which grow with θ_0, are larger. The inclination angle corresponding to the Galactic supermassive black hole is also expected to lie close to $\pi/2$. In this most simple case, we have

$$\alpha = -\frac{\Delta}{\Delta + a^2 h}\xi, \tag{19}$$

$$\beta = \pm\sqrt{\eta}. \tag{20}$$

For the visualization of the shape of the black hole shadow, one needs to plot β vs α. In Fig. 4, we show the contour of the shadows of black holes with rotation

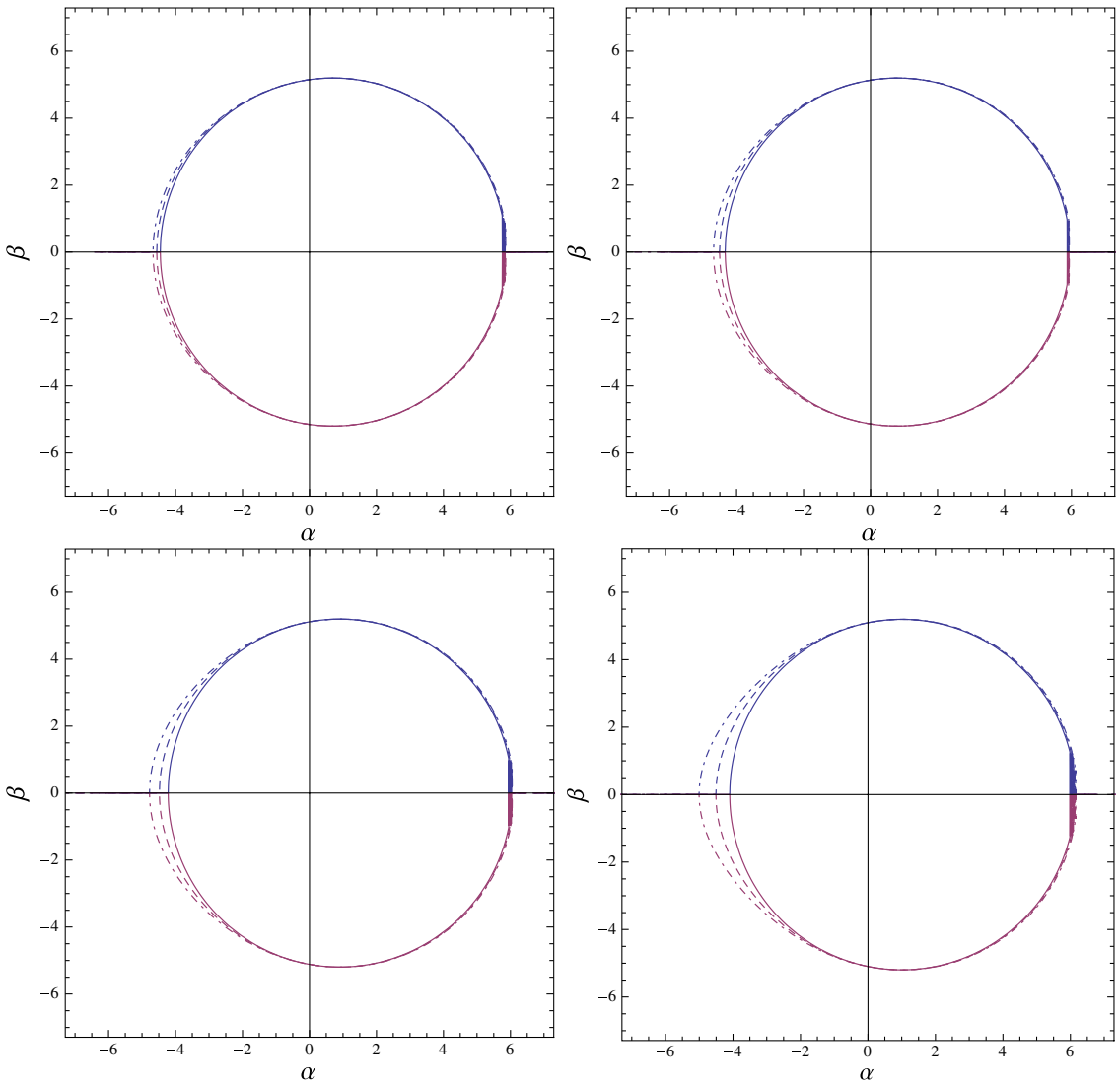

FIG. 4 (color online). Silhouette of the shadow cast by a non-Kerr black hole situated at the origin of coordinates with inclination angle $\theta = \pi/2$, having a rotation parameter a and a deformation parameter ϵ. Upper row, left: $a/M = 0.35$, $\epsilon = 0$ (solid line), $\epsilon = -5$ (dashed line), and $\epsilon = -10$ (dashed-dotted line). Upper row, right: $a/M = 0.4$, $\epsilon = 0$ (solid line), $\epsilon = -5$ (dashed line), and $\epsilon = -10$ (dashed-dotted line). Lower row, left: $a/M = 0.45$, $\epsilon = 0$ (solid line), $\epsilon = -5$ (dashed line), and $\epsilon = -10$ (dashed-dotted line). Lower row, right: $a/M = 0.5$, $\epsilon = 0$ (solid line), $\epsilon = -5$ (dashed line), and $\epsilon = -10$ (dashed-dotted line). The shadow corresponds to each curve and the region inside it.

parameters $a = 0.35$ (upper row, left), $a = 0.4$ (upper row, right), $a = 0.45$ (lower row, left), and $a = 0.5$ (lower row, right) for several values of the deformation parameter $\epsilon < 0$. In Fig. 5, we show the contour of the shadows of black holes with rotation parameters $a = 0.4$ (upper row, left), $a = 0.5$ (upper row, right), $a = 0.55$ (lower row, left), and $a = 0.6$ (lower row, right) for several values of the deformation parameter $\epsilon > 0$. From Figs 4 and 5, one can see that with increasing deformation parameter ($\epsilon > 0$), the shadow of the black hole decreases. This phenomena is also related to the fact that the increase of the deformation parameter forces photon orbits to come closer, which corresponds to the decrease of the gravitational force acting on photons. Photons with a smaller impact parameter could escape from absorbtion by the black hole in the presence of positive parameter ϵ. In the case of negative ϵ, the deflected photons with a particular value of impact parameter could be absorbed by a central object while they could escape in the pure Kerr black hole case with the same impact parameter. This of course corresponds to increasing the gravitational potential of the deformed rotating black hole in the case of the negative value of the deformation parameter.

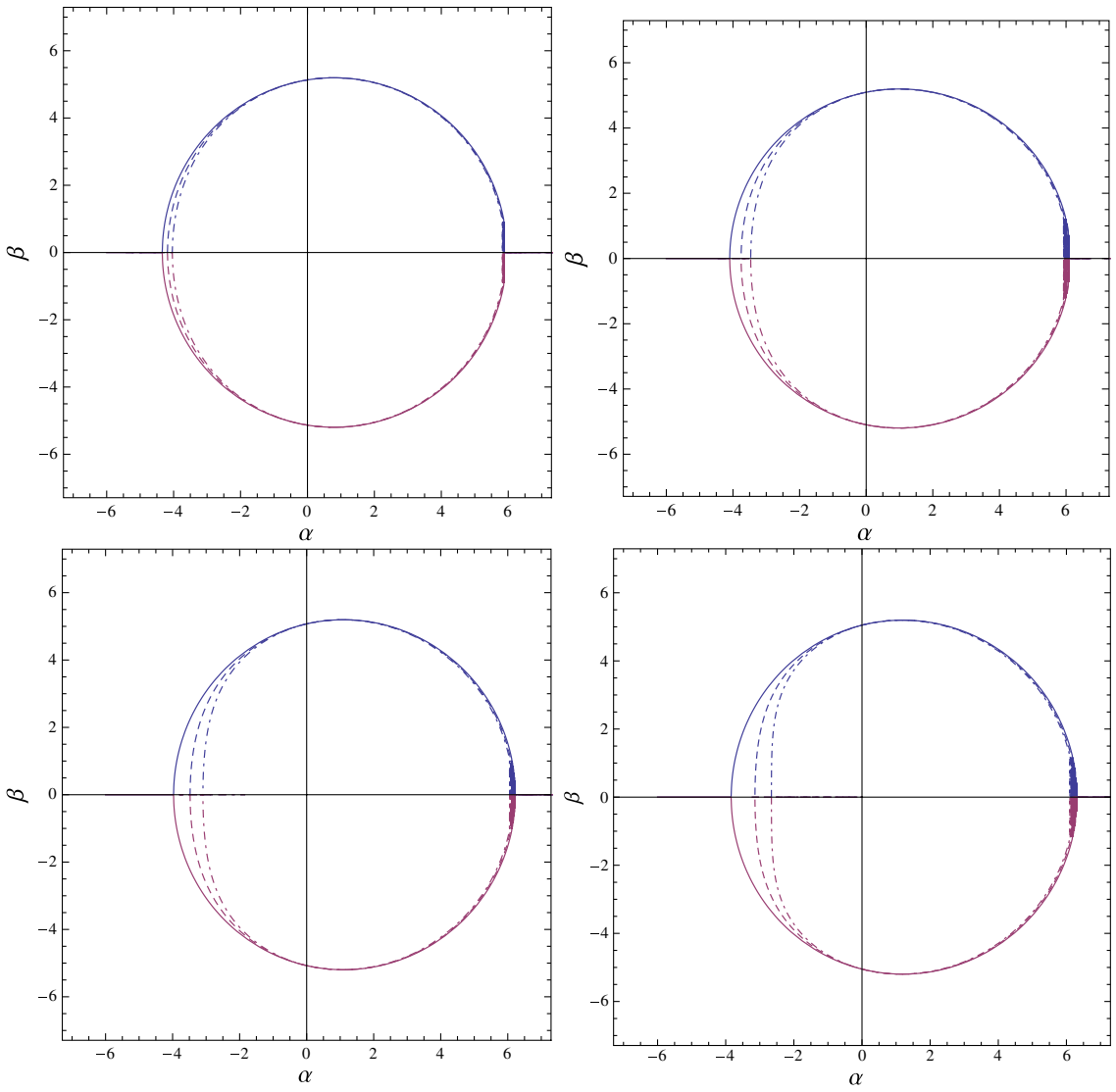

FIG. 5 (color online). Silhouette of the shadow cast by a non-Kerr black hole situated at the origin of coordinates with inclination angle $\theta = \pi/2$, having a rotation parameter a and a deformation parameter ϵ. Upper row, left: $a/M = 0.4$, $\epsilon = 0$ (solid line), $\epsilon = 5$ (dashed line), and $\epsilon = 10$ (dashed-dotted line). Upper row, right: $a/M = 0.5$, $\epsilon = 0$ (solid line), $\epsilon = 5$ (dashed line), and $\epsilon = 10$ (dashed-dotted line). Lower row, left: $a/M = 0.55$, $\epsilon = 0$ (solid line), $\epsilon = 5$ (dashed line), and $\epsilon = 10$ (dashed-dotted line). Lower row, right: $a/M = 0.6$, $\epsilon = 0$ (solid line), $\epsilon = 5$ (dashed line), and $\epsilon = 10$ (dashed-dotted line). The shadow corresponds to each curve and the region inside it.

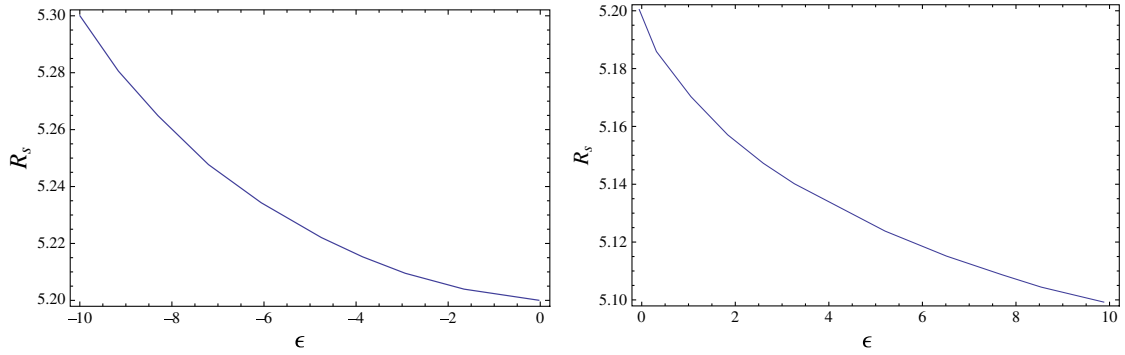

FIG. 6 (color online). Observables R_s as functions of the $\epsilon < 0$ and $\epsilon > 0$ parameters, corresponding to the shadow of a black hole situated at the origin of coordinates with inclination angle $\theta = \pi/2$ and spin parameters $a = 0.5$.

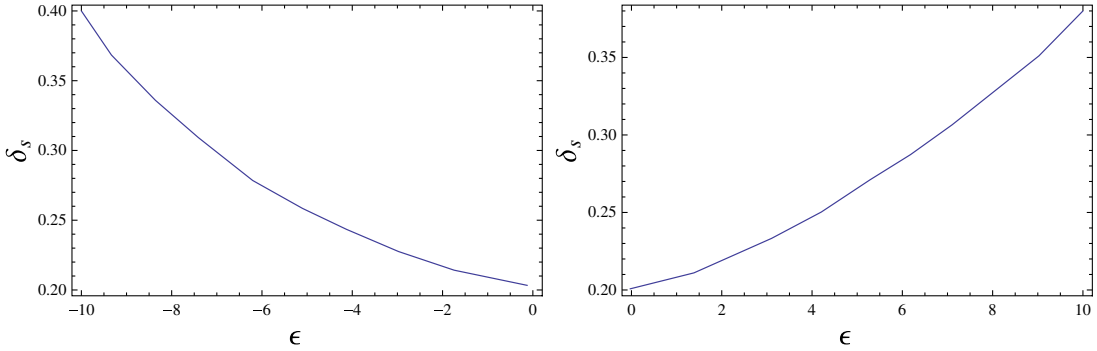

FIG. 7 (color online). Observables δ_s as functions of the $\epsilon < 0$ and $\epsilon > 0$ parameters, corresponding to the shadow of a black hole situated at the origin of coordinates with inclination angle $\theta = \pi/2$ and spin parameters $a = 0.5$.

The observable R_s can be calculated from the equation

$$R_s = \frac{(\alpha_t - \alpha_r)^2 + \beta_t^2}{2|\alpha_t - \alpha_r|},$$

and the observable δ_s is given by

$$\delta_s = \frac{\tilde{\alpha}_p - \alpha_p}{R_s},$$

where $(\tilde{\alpha}_p, 0)$ and $(\alpha_p, 0)$ are the points where the reference circle and the contour of the shadow cut the horizontal axis at the opposite side of $(\alpha_r, 0)$, respectively. In Fig. 6, the observables R_s as functions of the deformation parameter ϵ are shown for the value of the spin parameter of the black hole $a = 0.5$. In Fig. 7, the observable δ_s as a function of the deformation parameter ϵ is shown for the value of the spin parameter of the black hole $a = 0.5$. From these figures one may conclude that with the increase of the deformation parameter, the mean value of the shape of the shadow is decreasing. The increase of δ_s with the increase of the module of deformation parameter ϵ corresponds to the deviation of the shape of shadows from the pure circle. The deformed rotating black hole's shadow is also going to be deformed independently on the sign of deformation parameter.

IV. ROTATION OF POLARIZATION VECTOR FOR NON-KERR BLACK HOLE

In order to analyze possible effects of the parameters of non-Kerr gravity in terms of measurable quantities, we focus on geometrical optics of the light propagating around rotating non-Kerr black hole. The approach employed here was presented in Ref. [45] where the Newman-Penrose formalism was used to calculate optical quantities in the weak-field approximation with $a \ll M$.

The equations which govern the tangent vector k^μ (the wave vector) to the null congruence and the polarization vector f^μ are

$$k^\mu k_\mu = 0, \qquad Dk^\mu = 0, \tag{21}$$

and

$$k^\mu f_\mu = 0, \qquad Df^\mu = 0, \tag{22}$$

with the operator D denoting a covariant derivative in the k^μ direction.

In the Newman-Penrose formalism [39], a null tetrad is adopted, $\{e_{a\mu}\} = (m_\mu, \bar{m}_\mu, l_\mu, k_\mu)$, with the vector m_μ given by

$$m^\mu = \frac{\sqrt{2}}{2}(a^\mu + ib^\mu). \tag{23}$$

The vector m_μ is particularly relevant to the work developed here, as will be seen. An important feature of the formalism is that the k^μ direction is preserved under null rotations as

$$k'^\mu = Ak^\mu, \tag{24}$$

$$m'^\mu = e^{-i\chi}(m^\mu + Bk^\mu), \tag{25}$$

$$l'^\mu = A^{-1}(l^\mu + B\bar{m}^\mu + \bar{B}m^\mu + B\bar{B}k^\mu), \tag{26}$$

with $A > 0$, B complex, and χ real. The Newman-Penrose formalism provides 12 constants, the spin coefficients to the characterization of the spacetime. Some coefficients will be used to estimate the variation of the polarization vector in a rotating non-Kerr black hole background.

As shown in Ref. [39] when k^μ is tangent to the null congruence, the spin coefficient $\kappa \equiv -Dk_\mu m^\mu$ is zero. Moreover, considering that the null tetrad must parallelly propagate along the null congruence, this assumption implies that the other two spin coefficients vanish: $\varrho = \pi = 0$. Then the plane spanned by k^μ and a^μ can be identified with the polarization plane, which is parallelly propagated in the k^μ direction. That is, the polarization vector can be identified with the a^μ vector of the Newman-Penrose formalism. From this one can build an orthonormal frame

$$\{\mathbf{e}_a{}^{(\mu)}\} = \{r^{(\mu)}, \bar{r}^{(\mu)}, q^{(\mu)}, p^{(\mu)}\}, \tag{27}$$

such that this tetrad corresponds to the one-forms $\sigma^{(0)} = e^\nu dt$, $\sigma^{(1)} = e^\lambda dr$, $\sigma^{(2)} = e^\mu d\theta$, and $\sigma^{(3)} = (d\phi - \Omega dt)e^\psi$ of the locally nonrotating frame (LNRF) (the LNRF indices are indicated between parenthesis) [40]. For the spacetime metric given by Eq. (1), the expressions for e^ν, e^λ, e^μ, and e^ψ are presented in the Appendix A, Eq. (A2). Therefore, if the source and the observer are at rest with respect to the LNRF, they are dragged by rotation of the black hole. In Ref. [38] this construction was made, with the expression for the $m_+^{(\mu)}$ vector (i.e., a^μ)—the projection of m^μ on the LNRF—given by

$$a_+{}^{(\mu)} = \frac{1}{\sqrt{2}}\left\{0, -\frac{k^{(2)}}{k^{(0)}}, 1 - K(k^{(2)})^2, Kk^{(2)}k^{(3)}\right\}, \tag{28}$$

$$b_+{}^{(\mu)} = \frac{1}{\sqrt{2}}\left\{0, -\frac{k^{(3)}}{k^{(0)}}, -Kk^{(2)}k^{(3)}, 1 - K(k^{(3)})^2\right\}, \tag{29}$$

where $K = 1/[k^{(0)}(k^{(0)} + k^{(1)})]$ and $k^{(\mu)}$ is the projection of k^μ on the LNRF according to Eq. (A1). A null rotation was performed

$$m_+^{(\mu)} \rightarrow m^{(\mu)} = e^{-i\chi}m_+^{(\mu)}, \tag{30}$$

such that $\varrho = 0$. With this choice and considering the ϱ coefficient as $\varrho \equiv Dm_\mu \bar{m}^\mu/2$, it is shown that

$$D\chi = -2i\varrho_+. \tag{31}$$

Expression (31) indicates how the χ angle varies in the k^μ direction, i.e., the congruence direction. This variation will be important to calculate the variation of the polarization vector in that direction. For the spacetime metric (1), we obtain

$$\begin{aligned} D\chi &= -2i\varrho_+ \\ &= \frac{(\Gamma^{(t)}{}_{(\theta)(t)}k^{(t)} + \Gamma^{(r)}{}_{(\theta)(r)}k^{(r)} + \Gamma^{(r)}{}_{(\theta)(\theta)}k^{(\theta)} + \Gamma^{(t)}{}_{(\theta)(\phi)}k^{(\phi)})k^{(\phi)}}{k^{(t)} + k^{(r)}} \\ &\quad - \frac{(\Gamma^{(r)}{}_{(\phi)(t)}k^{(t)} + \Gamma^{(t)}{}_{(\phi)(r)}k^{(r)} + \Gamma^{(t)}{}_{(\phi)(\theta)}k^{(\theta)} + \Gamma^{(r)}{}_{(\phi)(\phi)}k^{(\phi)})k^{(\theta)}}{k^{(t)} + k^{(r)}} + \Gamma^{(\theta)}{}_{(\phi)(\phi)}k^{(\phi)} + \Gamma^{(\theta)}{}_{(\phi)(t)}k^{(t)}, \end{aligned} \tag{32}$$

$$D\chi = -D\chi(\cos\theta) + D\chi', \tag{33}$$

$$\begin{aligned} D\chi' &= \frac{1}{b}\left[\frac{P}{\sqrt{f}} - \frac{N}{1+h} + \frac{Q(a^2r^6(1+h)^2 + 3r^8(1+2h))}{\Delta + ha^2} - \frac{N(-2r^6 + a^2(2Mr^3 + 8M^4\epsilon + 3M^3r\epsilon))}{2r^8(1+h)}\right] \\ &\quad \times \left[\frac{\sqrt{b\Delta + jr^3(1+h)}}{\Delta r^3} + \frac{e\sqrt{\Delta(1+h)}}{(\Delta + ha^2)\sqrt{rf}}\right]^{-1} \sin\theta \frac{d\theta}{d\mu}, \end{aligned} \tag{34}$$

where

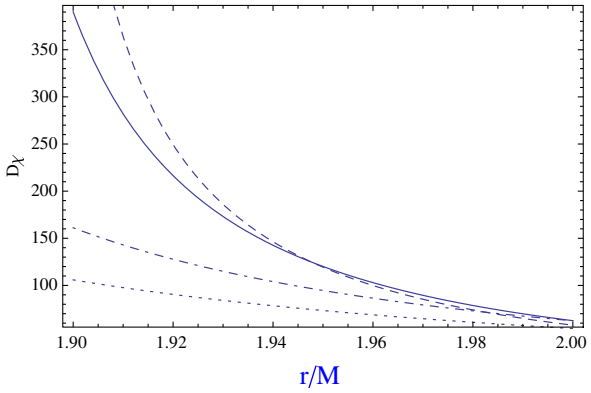

FIG. 8 (color online). The radial dependence of the polarization vector for the different values of the deformation parameter ϵ : solid line for $\epsilon = 0$, dashed line for $\epsilon = -1$, dotted-dashed line for $\epsilon = 5$, and dotted line for $\epsilon = 10$. $a = 0.5$.

$$b = \mathcal{L} - a\mathcal{E}, \qquad d = 2aM\mathcal{E} + \mathcal{L}(-2M + r),$$
$$f = r^3 + a^2(2M + r)(1 + h),$$
$$e = -2Ma\mathcal{L} + \mathcal{E}r^3 + a^2\mathcal{E}(2M + r),$$
$$j = (a\mathcal{L} - \mathcal{E}(a^2 + r^2))^2,$$
$$P = \frac{abMe}{r^2}\sqrt{\frac{\Delta}{r^3}},$$
$$N = \frac{fd}{r^3}, \qquad Q = \frac{aM}{r^9}\sqrt{\frac{b}{\Delta}}. \tag{35}$$

The expression in Eq. (33) is associated with the variation between $a^{(\mu)}$ and ${a_+}^{(\mu)}$ according to the null rotation indicated in Eq. (30).

The total variation of polarization vector taking into account Eq. (33) and the spacetime dragging is given by

$$\Delta\sigma = \Delta\chi + \Delta\phi. \tag{36}$$

The second term in right hand side of Eq. (36) is due to the spacetime dragging. The first term is obtained with the integration of $D\chi$ in Eq. (33) with respect to the ψ coordinate (see Ref. [38]), which plays the role of the azimuthal angle in the orbital plane of the null congruence. Moreover, a new angle was defined: α is the angle of the orbital plane with respect to the equatorial plane. That is, $\sin\alpha = \cos\theta\sin\psi$, and Eq. (33) is reduced to

$$D\chi' = \frac{1}{b}\left[\frac{P}{\sqrt{f}} - \frac{N}{1+h} + \frac{Q(a^2r^6(1+h)^2 + 3r^8(1+2h))}{\Delta + ha^2} - \frac{N(-2r^6 + a^2(2Mr^3 + 8M^4\epsilon + 3M^3r\epsilon))}{2r^8(1+h)}\right] \times \left[\frac{\sqrt{b\Delta + jr^3(1+h)}}{\Delta r^3} + \frac{e\sqrt{\Delta(1+h)}}{(\Delta + ha^2)\sqrt{rf}}\right]^{-1} \times \sin\alpha\frac{d(\sin\psi)}{d\mu}. \tag{37}$$

Here we have found the dependence of the polarization vector from parameter ϵ in equatorial plane ($\theta = \pi/2$). In Fig. 8 the radial dependence of the polarization vector is shown for the different values of deformation parameter ϵ. From the dependence one can easily see that presence of the parameter ϵ due to non-Kerr modification decreases the polarization angle. This dependence may help to get constraints on parameter ϵ from observational data related to the geometrical optics features of compact objects.

V. CONCLUSIONS

In this paper we have studied the optical features of rotating non-Kerr (deformed) black hole. It was shown that with the increase of the deformation parameter, the shape of the effective potential is going to be shifted to the central object. The stability of photon orbits will also increase with the increasing parameter ϵ.

We have analyzed how the shadow of the black hole is distorted by the presence of the deformation parameter ϵ. We have shown that with increasing deformation parameter ($\epsilon > 0$), the radius of the shadow of the black hole decreases. This phenomena is also related to the fact that the increase of the deformation parameter forces photon orbits to come closer, which corresponds to the decrease of the gravitational force acting on photons. In the case of negative ϵ, the deflected photons with a particular value of impact parameter could be absorbed by the central object while they could escape in the pure Kerr black hole case with the same impact parameter. The increase of distortion parameter δ_s with the increase of the module of deformation parameter ϵ corresponds to the deviation of the shape of shadows from the pure circle. The deformed rotating black hole's shadow is also going to be deformed independently on the sign of the deformation parameter.

Since black hole's shadows give the region where one can never observe any light from the gravitational source, one should look for a part of the shape of the realistic light source [18]. In the near future, if the instrumental astronomy would give more accurate measurements, at least, on the part of the black hole's shape, one can find constraints on deformation parameter ϵ in non-Kerr spacetime.

The recent measurements of the gravitational lens systems [46] may give alternate constraints on the numerical values of the deformation parameter ϵ in the rotating non-Kerr black hole. Astrophysical quantities related to the observable properties of the polarization vector can be obtained from the spacetime metric, and in turn observations have provided important information about the ϵ parameter. To get the estimation for the value of deformation parameter ϵ, one should compare the observational results with the obtained theoretical results on the polarization angle. For the nuclei of spiral galactic systems B0218 + 357 and PKS1830 − 211, the differential polarization angles have been found to be $913 \pm 31\ \mathrm{rad\,m^{-2}}$ and $1480 \pm 83\ \mathrm{rad\,m^{-2}}$, respectively, from the observed

correlation of the Faraday rotation measurements [47]. Since the effect of the deformation parameter ϵ is within the error of the observation, we may put $D\chi(\epsilon \neq 0)/D\chi(\epsilon = 0) = 1 + \zeta$, where ζ is the relative error of the observation. Putting the value of ζ from the observations [47] into the above condition, one can easily make an estimation on the upper limit for the deformation parameter ϵ as $\epsilon \leq 19$.

ACKNOWLEDGMENTS

Authors thank the Max-Planck-Institut für Gravitationsphysik (Albert-Einstein-Institut), Potsdam-Golm, Germany for warm hospitality. A. A. and B. A. thank the TIFR, IUCAA (India), and Faculty of Philosophy and Science, Silesian University in Opava (Czech Republic) for warm hospitality. This research is supported in part by the Projects No. F2-FA-F113, No. FE2-FA-F134, and No. F2-FAF029 of the UzAS, by the ICTP through Projects No. OEA-NET-76 and No. OEA-PRJ-29, and the Volkswagen Stiftung.

APPENDIX A: QUANTITIES IN THE LOCALLY NONROTATING FRAME

All physical quantities are indicated by parenthesis around the Greek indices in the (LNRF). The components of $k^\mu = dx^\mu/d\mu = \dot{x}^\mu$, which is tangent to the null congruence and its projections $k^{(\mu)}$ on the LNRF, are

$$\begin{aligned} k^{(0)} &= k^{(t)} = e^{\nu} k^0 = e^{\nu}\dot{t}, \\ k^{(1)} &= k^{(r)} = e^{\lambda} k^1 = e^{\lambda}\dot{r}, \\ k^{(2)} &= k^{(\theta)} = e^{\mu} k^2 = e^{\mu}\dot{\theta}, \\ k^{(3)} &= k^{(\phi)} = e^{\psi}(k^3 - \Omega k^0) = e^{\psi}(\dot{\phi} - \Omega\dot{t}), \\ \Omega &= \frac{2Mar(1+h)}{A}. \end{aligned} \tag{A1}$$

The functions ν, λ, μ, and ψ are listed as the following:

$$\begin{aligned} e^{2\nu} &= \frac{\Sigma^2\Delta(1+h)}{A}, \\ e^{2\lambda} &= \frac{\Sigma^2(1+h)}{\Delta + a^2 h \sin^2\theta}, \\ e^{2\mu} &= \Sigma^2, \\ e^{2\psi} &= \frac{\sin^2\theta}{\Sigma^2 A}, \\ A &= \Sigma^4 + a^2(\Sigma^2 + 2Mr)(1+h)\sin^2\theta. \end{aligned} \tag{A2}$$

The nonzero components of the connection projected on the LNRF [40] are

$$\begin{aligned} \Gamma^{(t)}_{(r)(t)} &= \Gamma^{(r)}_{(t)(t)} = \partial_r \nu e^{-\lambda}, \\ \Gamma^{(t)}_{(\theta)(t)} &= \Gamma^{(\theta)}_{(t)(t)} = \partial_\theta \nu e^{-\mu}, \\ \Gamma^{(r)}_{(\theta)(r)} &= -\Gamma^{(\theta)}_{(r)(r)} = \partial_\theta \lambda e^{-\mu}, \\ \Gamma^{(r)}_{(\theta)(\theta)} &= -\Gamma^{(\theta)}_{(r)(\theta)} = -\partial_r \mu e^{-\lambda}, \\ \Gamma^{(r)}_{(\phi)(\phi)} &= -\Gamma^{(\phi)}_{(r)(\phi)} = -\partial_r \psi e^{-\lambda}, \\ \Gamma^{(\theta)}_{(\phi)(\phi)} &= -\Gamma^{(\phi)}_{(\theta)(\phi)} = -\partial_\theta \psi e^{-\mu}, \\ \Gamma^{(t)}_{(r)(\phi)} &= \Gamma^{(r)}_{(t)(\phi)} = \Gamma^{(t)}_{(\phi)(r)} = \Gamma^{(r)}_{(\phi)(t)} = -\Gamma^{(\phi)}_{(t)(r)} = -\Gamma^{(\phi)}_{(r)(t)} \\ &= \frac{1}{2}\partial_r \Omega e^{\psi-\nu-\lambda}, \end{aligned}$$

$$\begin{aligned} \Gamma^{(t)}_{(\theta)(\phi)} &= \Gamma^{(\theta)}_{(t)(\phi)} = \Gamma^{(t)}_{(\phi)(\theta)} = \Gamma^{(\theta)}_{(\phi)(t)} = -\Gamma^{(\phi)}_{(t)(\theta)} = -\Gamma^{(\phi)}_{(\theta)(t)} \\ &= \frac{1}{2}\partial_\theta \Omega e^{\psi-\nu-\mu}. \end{aligned} \tag{A3}$$

[1] P. Hořava, J. High Energy Phys. 03 (2009) 020; Phys. Rev. D **79**, 084008 (2009).
[2] S. Deser and B. Tekin, Phys. Rev. Lett. **89**, 101101 (2002); Phys. Rev. D **67**, 084009 (2003).
[3] L. Randall and R. Sundrum, Phys. Rev. Lett. **83**, 3370 (1999); N. K. Dadhich, R. Maartens, P. Papodopoulos, and V. Rezania, Phys. Lett. B **487**, 1 (2000); R. Maartens, Living Rev. Relativity **7**, 7 (2004).
[4] T. Johannsen and D. Psaltis, Astrophys. J. **716**, 187 (2010); T. A. Apostolatos, G. Lukes-Gerakopoulos, and G. Contopoulos, Phys. Rev. Lett. **103**, 111101 (2009); C. Bambi, F. Caravelli, and L. Modesto, Phys. Lett. B **711**, 10 (2012); P. Pani, C. F. B. Macedo, L. C. B. Crispino, and V. Cardoso, Phys. Rev. D **84**, 087501 (2011).
[5] T. Johannsen and D. Psaltis, Phys. Rev. D **83**, 124015 (2011).
[6] S. N. Zhang, W. Cui, and W. Chen, Astrophys. J. **482**, L155 (1997); L.-X. Li, E. R. Zimmerman, R. Narayan, and J. E. McClintock, Astrophys. J. Suppl. Ser. **157**, 335 (2005); J. E. McClintock, R. Narayan, S. W. Davis, L. Gou, A. Kulkarni, J. A. Orosz, R. F. Penna, R. A. Remillard, and J. F. Steiner, Classical Quantum Gravity **28**, 114009 (2011).
[7] C. Bambi, Phys. Rev. D **85**, 043002 (2012).
[8] C. Liu, S. Chen, and J. Jing, Astrophys. J. **751**, 148 (2012).
[9] C. Bambi, F. Caravelli, and L. Modesto, Phys. Lett. B **711**, 10 (2012).
[10] S. Chen and J. Jing, Phys. Rev. D **85**, 124029 (2012).

[11] H. Krawczynski, Astrophys. J. **754**, 133 (2012).
[12] C. Bambi, Mod. Phys. Lett. A **26**, 2453 (2011).
[13] C. Bambi and E. Barausse, Phys. Rev. D **84**, 084034 (2011).
[14] J. M. Bardeen, in *Black Holes*, Proceedings of the Les Houches Summer School, Session 215239, edited by C. De Witt and B. S. De Witt (Gordon and Breach, New York, 1973).
[15] J.-P. Luminet, Astron. Astrophys. **75**, 228 (1979).
[16] N. Quien, R. Wehrse, and C. Kindl, Spektrum der Wissenschaft **5**, 5667 (1995).
[17] A. de Vries, Classical Quantum Gravity **17**, 123 (2000).
[18] K. Hioki, and K. I. Maeda, Phys. Rev. D **80**, 024042 (2009).
[19] B. C. Bromley, F. Melia, and S. Liu, Astrophys. J. **555**, L83 (2001); A. de Vries, Phys. Unserer Zeit **35**, 128 (2004); H. Falcke, F. Melia, and E. Agol, Astrophys. J. **528**, L13 (2000)
[20] C. Darwin, Proc. R. Soc. A **249**, 180 (1959).
[21] H. C. Ohanian, Am. J. Phys. **55**, 428 (1987); R. J. Nemiroff, Am. J. Phys. **61**, 619 (1993); V. Bozza, S. Capozziello, G. Iovane, and G. Scarpetta, Gen. Relativ. Gravit. **33**, 1535 (2001).
[22] A. A. Abdujabbarov, F. S. Atamurotov, Y. Kucukakca, B. J. Ahmedov, and U. Camci, Astrophys. Space Sci. **344**, 429 (2013).
[23] E. F. Eiroa, G. E. Romero, and D. F. Torres, Phys. Rev. D **66**, 024010 (2002).
[24] V. Bozza, Phys. Rev. D **66**, 103001 (2002).
[25] S. Pal and S. Kar, Classical Quantum Gravity **25**, 045003 (2008); V. Frolov, M. Snajdr, and D. Stojkovic, Phys. Rev. D **68**, 044002 (2003); E. F. Eiroa, Phys. Rev. D **71**, 083010 (2005); R. Whisker, Phys. Rev. D **71**, 064004 (2005); A. S. Majumdar and N. Mukherjee, Int. J. Mod. Phys. D **14**, 1095 (2005); E. F. Eiroa, Braz. J. Phys. **35**, 1113 (2005); C. R. Keeton and A. O. Petters, Phys. Rev. D **73**, 104032 (2006); A. Y. Bin-Nun, Phys. Rev. D **81**, 123011 (2010); **82**, 064009 (2010).
[26] L. Amarilla and E. F. Eiroa, Phys. Rev. D **85**, 064019 (2012).
[27] V. Bozza, Phys. Rev. D **67**, 103006 (2003); V. Bozza, F. De Luca, G. Scarpetta, and M. Sereno, Phys. Rev. D **72**, 083003 (2005); V. Bozza, F. De Luca, and G. Scarpetta, Phys. Rev. D **74**, 063001 (2006).
[28] S. E. Vazquez and E. P. Esteban, Nuovo Cimento Soc. Ital. Fis. **119B**, 489 (2004).
[29] V. Bozza and G. Scarpetta, Phys. Rev. D **76**, 083008 (2007).
[30] G. V. Kraniotis, Classical Quantum Gravity **28**, 085021 (2011).
[31] J. Bardeen, *Black Holes*, Proceedings of the Les Houches Summer School, edited by C. De Witt and B. S. De Witt (Gordon and Breach, New York, 1973).
[32] S. Chandrasekhar, *The Mathematical Theory of Black Holes* (Oxford University, New York, 1992).
[33] H. Falcke, F. Melia, and E. Agol, Astrophys. J. **528**, L13 (2000).
[34] L. Amarilla, E. F. Eiroa, and G. Giribet, Phys. Rev. D **81**, 124045 (2010).
[35] A. F. Zakharov, A. A. Nucita, F. De Paolis, and G. Ingrosso, New Astron. **10**, 479 (2005); A. F. Zakharov, F. De Paolis, G. Ingrosso, and A. A. Nucita, Astron. Astrophys. **442**, 795 (2005); F. De Paolis, G. Ingrosso, A. A. Nucita, A. Qadir, and A. F. Zakharov, Gen. Relativ. Gravit. **43**, 977 (2011); G. Ingrosso, S. Calchi Novati, F. De Paolis, Ph. Jetzer, A. A. Nucita, F. Strafella, and A. F. Zakharov, Mon. Not. R. Astron. Soc. **426**, 1496 (2012); A. F. Zakharov, F. De Paolis, G. Ingrosso, and A. A. Nucita, New Astron. Rev. **56**, 64 (2012).
[36] J. Schee and Z. Stuchlik, Int. J. Mod. Phys. D **18**, 983 (2009).
[37] V. Bozza, Gen. Relativ. Gravit. **42**, 2269 (2010).
[38] S. Pineault and R. C. Roeder, Astrophys. J. **212**, 541 (1977).
[39] E. Newman and R. Penrose, J. Math. Phys. (N.Y.) **3**, 566 (1962).
[40] J. M. Bardeen, W. H. Press, and S. A. Teukolsky. Astrophys. J. **178**, 347 (1972).
[41] R. Beig, Gen. Relativ. Gravit. **12**, 439 (1980); R. Beig and W. Simon, Proc. R. Soc. A **376**, 333 (1981).
[42] C. M. Will, Living Rev. Relativity **9**, 3 (2006).
[43] J. G. Williams, S. G. Turyshev, and D. H. Boggs, Phys. Rev. Lett. **93**, 261101 (2004).
[44] A. A. Abdujabbarov, B. J. Ahmedov, and N. B. Jurayeva, Phys. Rev. D **87**, 064042 (2013).
[45] J. C. S. Neves and C. Molina, Phys. Rev. D **86**, 124047 (2012); S. Pineault and R. C. Roeder, Astrophys. J. **212**, 541 (1977).
[46] P. E. Greenfield, D. H. Roberts, and B. F. Burke, Astrophys. J. **293**, 370 (1985); A. R. Patnaik, A. J. Kemball, R. W. Porcas, and M. A. Garrett, Mon. Not. R. Astron. Soc. **307**, L1 (1999); L. J. King, I. W. A. Browne, T. W. B. Muxlow, D. Narasimha, A. R. Patnaik, R. W. Porcas, and P. N. Wilkinson, Mon. Not. R. Astron. Soc. **289**, 450 (1997); G. H. Chen and J. N. Hewitt, Astrophys. J. **106**, 1719 (1993).
[47] A. R. Patnaik, K. H. Menten, R. W. Porcas, and A. J. Kembal, Mon. Not. R. Astron. Soc. **261**, 435 (1993); R. Subrahmanyan, D. Narasimha, A. P. Rao, and G. J. Swarup, Mon. Not. R. Astron. Soc. **246**, 263 (1990).